Discrete Models of Autocrine Cell Communication in Epithelial Layers

M. Pribyl[(1)], C. B. Muratov[(2)] and S. Y. Shvartsman[(1)]

[(1)] Department of Chemical Engineering and
Lewis-Sigler Institute for Integrative Genomics
Princeton University, Princeton, NJ 08544

[(2)] Department of Mathematical Sciences and
Center for Applied Mathematics and Statistics
New Jersey Institute of Technology, Newark, NJ 07102

CAMS Report 0203-16, Spring 2003

Center for Applied Mathematics and Statistics

NJIT

DISCRETE MODELS OF AUTOCRINE CELL COMMUNICATION IN EPITHELIAL LAYERS

Michal Přibyl[1], Cyrill B. Muratov[2], and Stanislav Y. Shvartsman[1]

[1]Department of Chemical Engineering and Lewis-Sigler Institute for Integrative Genomics, Princeton University

[2]Department of Mathematical Sciences and Center for Applied Mathematics and Statistics, New Jersey Institute of Technology

Corresponding Author:

Stanislav Y. Shvartsman

Department of Chemical Engineering and Lewis-Sigler Institute for Integrative Genomics, Princeton University

Tel: 609-258-4694; Fax: 609-258-0211

Princeton, NJ 08544, stas@princeton.edu

Keywords: epithelial layers, cell communication, ligand, receptor, transport, signaling, pattern formation, modeling, discrete.

Running title: Cell communication in epithelial layers

Abstract

Pattern formation in epithelial layers heavily relies on cell communication by secreted ligands. While the experimentally observed signaling patterns can be visualized at single cell resolution, a biophysical framework for their interpretation is currently lacking. To this end, we develop a family of discrete models of cell communication in epithelial layers. The models are based on the introduction of cell-cell coupling coefficients that characterize the spatial range of intercellular signaling by diffusing ligands. We derive the coupling coefficients as functions of geometric, cellular, and molecular parameters of the ligand transport problem. Using these coupling coefficients, we analyze a nonlinear model of positive feedback between ligand release and binding. In particular, we study criteria of existence of the patterns consisting of clusters of a few signaling cells, as well as the onset of signal propagation. We use our model to interpret recent experimental studies of EGFR/Rhomboid/Spitz module in *Drosophila* development.

Introduction

Epithelial layers provide a common substrate for pattern formation in development (Hogan 1999; Shilo 2001). In general, cell-cell communication produces spatially nonuniform patterns in the expression of genes that guide the development of tissues and organs. The design principles of epithelial patterning are being formulated only now (Freeman and Gurdon 2002). An important family of epithelial patterning mechanisms relies on secreted chemical signals. Typically, a ligand released by a group of cells interacts with the extracellular matrix and cell surface receptors as it spreads through the tissue. Ligand transport can be integrated with positive and negative intracellular feedback loops (Freeman 2000). For example, ligand-receptor binding can stimulate ligand synthesis and secretion (Freeman and Gurdon 2002; Stevens 1998). Ligand release can be regulated by the occupancy of cell surface receptors. Receptor occupancy, in turn, may be determined by the balance between ligand transport, binding, and degradation, Figure 1D.

Here, we consider a general problem of interaction between cells arranged in an epithelial layer and communicating by secreted ligands. The original motivation for the problem comes from *Drosophila* egg development (Spradling 1993), where pattern formation proceeds in the follicular epithelium - a layer of columnar epithelial cells that envelop the oocyte. Follicle cells are much smaller (5-7 μm) than the oocyte (100-300 μm), Figure 1A. Reciprocal oocyte/follicle cell interactions pattern the eggshell and establish the embryonic axes (Van Buskirk and Schupbach 1999). These events rely on the Epidermal

Growth Factor receptor (EGFR), a well-studied receptor tyrosine kinase (Nilson and Schupbach 1999; Wells 1999). EGFRs are uniformly distributed across the follicular epithelium and are absent on the oocyte surface (Sapir and others 1998). EGFR is activated by ligands secreted from the oocyte and from the follicle cells themselves. Secreted ligands diffuse in the thin (< 1 μm) gap between the follicle cells and the oocyte, Figure 1B. Release of EGFR ligands is regulated by the intracellular proteases (Urban and others 2002). Interestingly, the expression of these proteases (Rhomboids), is positively regulated by EGFR signaling (Hsu and others 2001; Peri and others 1999; Sapir and others 1998; Wasserman and Freeman 1998), Figure 1E. To summarize, ligands diffuse in a thin gap between receptor covered epithelium and a reflective surface; receptor activation stimulates further ligand release by activating the expression of the intracellular protease.

The significance of the EGFR-mediated positive feedback in *Drosophila* oogenesis is well-established (Barkai and Shilo 2002; Stevens 1998). Most importantly, the system can be both monitored and manipulated genetically. In particular, the spatial distribution of the ligand-releasing protease across the epithelium can be visualized at the mRNA and protein levels (Peri and others 1999; Sapir and others 1998; Wasserman and Freeman 1998). Similar signaling/transport arrangements are encountered later in fruit fly development and in other species, both for the EGFR and other signaling systems (Doraiswamy and others 2000; Freeman and Gurdon 2002).

The gene expression patterns in developing epithelial layers can be very fine-grained. In many cases, the width of the signaling patterns is only a couple of cells (Carmena and others 2002; Hasty and others 2002; Hatini and DiNardo 2001; Peri and others 1999; Ruohola-Baker and others 1993; Sapir and others 1998). What is the appropriate biophysical description for such systems? There have been several attempts to use continuum models for the analysis of such patterns, e.g., (Lander and others 2002; Shvartsman and others 2002). These models assume that the relevant length scale of the pattern is greater than the size of a single cell. The validity of such an assumption may be difficult to reconcile with the fine-grained nature of experimentally observed signaling patterns. Starting from the work of Othmer and Scriven, a number of discrete models for cellular layers has been proposed (Collier and others 1996; Meir and others 2002; Monk 1998; Othmer and Scriven 1971; Owen and others 1999; Owen and others 2000; von Dassow and others 2000). However, in these models the form of cell-cell couplings has been chosen on purely phenomenological grounds.

Here, we systematically derive discrete models of cell-cell communication from a mechanistic description of autocrine and paracrine signaling in epithelial layers. These models are discrete because they treat each cell individually. The models are also long-ranged: they use the state of the entire layer in describing the dynamics of each cell and thus take into account non-nearest neighbour cell-cell interactions. Our derivation is based on the introduction of coupling coefficients that characterize the communication of cells by secreted ligands. These coupling coefficients are directly linked to the biophysical parameters of the transport problem. Central to our approach is the use of the

separation of time scales between diffusing and intracellular species. We argue that binding and transport are fast and are therefore dynamically slaved to the slow intracellular variables when the intracellular processes involve transcription and protein synthesis. With the coupling coefficients at hand, we are then able to formulate discrete models that account for particular intracellular processes, such as receptor-mediated activation of ligand release, and study their properties associated with discreteness.

Description of the Mathematical Model

Our model accounts for the coupled dynamics of extracellular ligand, ligand-receptor complexes, and ligand-releasing proteases in each cell within the epithelial layer. In formulating the model, we assume that the system operates in the ligand limited regime and that the free receptors are in excess. This is supported by experiments in several model organisms (Freeman and Gurdon 2002). Following the standard receptor binding analysis, this approximation requires that the concentration of ligand is less than the equilibrium binding constant, $K_D = k_{off} / k_{on}$. With this in mind, a mechanistic model of transport and signaling in an idealized epithelium consisting of a two-dimensional periodic array of identical cells in a single flat layer geometry takes the following form (Figure 1B,D):

$$\frac{\partial S}{\partial t} = D\left(\frac{\partial^2 S}{\partial X^2} + \frac{\partial^2 S}{\partial Y^2} + \frac{\partial^2 S}{\partial Z^2}\right) \qquad (1)$$

$$\frac{\partial C}{\partial t} = k_{on} R_0 \bar{S} - \left(k_{off} + k_e \right) C, \quad \bar{S} = S\big|_{Z=0} \tag{2}$$

$$\frac{dP_{i,j}}{dt} = -k_p P_{i,j} + g_p \sigma \left(C_{i,j}^{tot} - C_T \right), \quad C_{i,j}^{tot} = \int_{A_{i,j}} C dX dY \tag{3}$$

$$\left(D \frac{\partial S}{\partial Z} - k_{on} R_0 S \right)\Big|_{Z=0} = -k_{off} C - \frac{g_r}{A} \sum_{i,j} \theta_{i,j} \left(X, Y \right) P_{i,j} \qquad \frac{\partial S}{\partial Z}\Big|_{Z=h} = 0 \tag{4}$$

Here, $S = S(X, Y, Z, t)$ is the concentration of ligand in the extracellular space, $C = C(X, Y, t)$ is the number of ligand-receptor complexes per unit area on the cell surfaces, $P_{i,j}(t)$ is the amount of ligand-releasing protease in the cell with index *i,j* (one index for each dimension of the two-dimensional cell lattice; for concrete indexing schemes in particular cell geometries see Appendix), *X* and *Y* are the coordinates in the plane of the epithelial layer, *Z* is the transverse coordinate, and *t* is time. $C_{i,j}^{tot}$ is the total number of ligand-receptor complexes on the surface of cell i,j. *D* is the diffusion coefficient of the ligand in the extracellular space, $k_{on} R_0$ is the product of the rate of ligand-receptor forward binding and the number of receptors per unit area, k_{off} is the ligand-receptor complex dissociation constant, k_e is the rate of ligand-induced receptor internalization.

Thus, equation 1 models the three-dimensional extracellular ligand diffusion in the gap of width *h* between the layer of cells and an impermeable barrier, while equation 2 describes the reversible ligand-receptor binding and the first-order receptor-mediated endocytosis (Burke and others 2001; Lauffenburger and Linderman 1993), Figure 1D. In the dynamic

balance for ligand-receptor complexes, $\overline{S}$ is the ligand concentration at the receptor-covered cell surfaces.

Similarly, equation 3 models the ligand-releasing protease dynamics in each cell within the epithelial layer. These dynamics consist of the combination of the first-order degradation characterized by rate constant k_p and a sigmoidal generation function $g_p\sigma(C_{i,j}^{tot} - C_T)$ characterized by the production rate g_p and the threshold C_T. Such parameterization lumps a number of processes and is common in modeling of regulatory networks (Bolouri and Davidson 2002; Ferrell 1997; Smolen and others 2000). In the following we choose $\sigma(x)$ to be the Heaviside function, thus assuming a sharp threshold; our results do not significantly depend on the precise form of $\sigma(x)$. Furthermore, our first order degradation combines the degradation at the mRNA and protein level. Let us emphasize that this threshold-like generation term is a function of the total number of ligand-receptor complexes $C_{i,j}^{tot}$ on the i,j-th cell. Therefore, it is related to the distribution of complexes by the integral over the area of the i,j-th cell surface (equation 3). This is supported by at least one direct measurement (Dyson and Gurdon 1998).

The boundary condition for equation 1 on the surface of the epithelial layer ($Z = 0$), which couples the diffusion of the ligand with its secretion (as a result of intracellular processes), is given by equation 4. It accounts for the reversible binding and protease-mediated ligand release. The source term in this boundary condition is spatially nonuniform and varies from cell to cell across the layer. There are two contributions to this term: dissociation of ligand-receptor complexes and protease-mediated ligand

release. The latter is assumed to be uniform over each cell's surface, which is expressed by the characteristic function $\theta_{i,j}(X,Y)$, which is equal to one on the surface of the i,j-th cell and zero elsewhere, and is regulated by the availability of the ligand-releasing protease. This assumption is supported by the antibody stainings that reveal uniform pattern of unprocessed Spitz in the follicle cells (Wasserman and Freeman 1998). Ligand release is modeled as first order with respect to the protease, with the release rate per cell given by $g_r P_{i,j}$ (A is the area of the cell surface). Ligand-precursor, on which the ligand-releasing protease is acting, is assumed to be in excess. At least for the EGFR system, these assumptions are supported by a large number of experiments (Dong and others 1999; Dong 1999; Sapir and others 1998; Urban and others 2002). There is also a no-flux boundary condition at the impermeable barrier (Z = h) in Equation 4.

Goals of the paper and plan of the analysis

The model describes the coupled dynamics of cells in an idealized epithelial layer. To characterize these dynamics, we need to track both the extracellular and intrcellular variables in the system of integrodifferential equations 1-4. We would like to quantify the spatial extent of cell-cell communication and to analyze the effect of this coupling on the dynamics of individual cells. As an application, we consider the consequences of activating ligand release in a small group of cells within the layer. Such perturbations are implemented using techniques for tissue specific gene expression and are routinely employed in developmental biology (Brand and Perrimon 1993; Duffy and others 1998).

Analysis of such perturbations requires models that can resolve individual cells. It is our goal to formulate such models.

Results

Main approximations

We consider the case when the height of the medium for ligand diffusion is small relative to the appropriately chosen dynamic length scale in the problem. In terms of the original model parameters, this translates into the following inequality $h \ll D/k_s$, where

$$k_s = k_e k_{on} R_0 /(k_{off} + k_e)$$

characterizes the steady state rate of ligand degradation. In this case, the spatial variation of the ligand field in the z-direction is negligible: $S(X,Y,Z,t) \cong S(X,Y,t)$. This approximation is expected to be very accurate for the chosen set of geometric and dynamic parameters.

In addition to reducing the number of spatial dimensions, we reduce the number of dependent variables. Our argument is based on the time-scale separation between the ligand dynamics and those of the intracellular protease. In our description, ligand binding stimulates the transcription of the ligand-releasing protease. Since this process happens on a time scale that is longer in comparison to those of binding, transport and endocytosis, we can set the time derivatives in the dynamic balances for extracellular and

receptor-bound ligand to zero. This approximation imposes the following constraints on the time scales: $k_p \ll k_{off} + k_e$ and $k_p \ll k_s^2 / D$ (see Appendix).

Together with the assumption of the ligand-limited regime, these approximations lead to the following reduced model:

$$0 = D\Delta S - \frac{1}{h}\left(k_s S - \frac{g_r}{A} \sum_{i,j} \theta_{i,j}(X,Y) P_{i,j} \right) \tag{5}$$

$$\frac{dP_{i,j}}{dt} = -k_p P_{i,j} + g_p \sigma \left(\frac{k_s}{k_e} \int_{A_{i,j}} S(X,Y,t) dX dY - C_T \right) \tag{6}$$

where $\Delta = \partial^2 / \partial X^2 + \partial^2 / \partial Y^2$.

Hence, the problem in Equations 1-4 is reduced to the equation for protease dynamics in individual cells coupled to the steady linear reaction-diffusion equation for extracellular ligand. The linear problem for the ligand field can be easily solved for any particular pattern of protease activity. Then, the resulting instantaneous field, $S(X,Y,t)$, can be integrated over the area of each cell to provide arguments for the protease generation function. This leads to a fully discrete model for cell communication. In the following, this program is implemented for square- and hexagonal-shaped cells. Before that, we rescale the problem and describe the dimensionless groups.

Nondimensionalization

Equations 5-6 are rendered dimensionless by the following transformations

$$\tau \equiv k_p t,\ x \equiv X/L,\ y \equiv Y/L,\ s \equiv S/S_0,\ p_{i,j} \equiv P_{i,j}/P_0, \tag{7}$$

where

$$P_0 = g_p/k_p,\ S_0 = g_r g_p/\left(Ak_p k_s\right),\ L = D/k_s. \tag{8}$$

For estimates of the relevant quantities, see Table 1.

Notice that P_0 and S_0 determine the maximum levels of protease and ligand concentrations. In fact, these values are attained when ligand release is at its maximal "on" level uniformly throughout the layer ($p_{i,j} = 1$ for all cells). Associated with these maximum values is the maximum level of ligand-receptor complexes $C_0 \equiv k_{on} R_0 S_0/(k_e + k_{off})$ and the maximum *total* number of ligand-receptor complexes per cell: $C_0^{tot} \equiv C_0 A$.

After rescaling, the problem takes the following form:

$$\alpha \Delta s - s + \sum_{ij} \theta_{i,j}(x,y)\, p_{i,j} = 0, \tag{9}$$

$$\frac{dp_{i,j}}{d\tau} = -p_{i,j} + \sigma\left(s_{i,j}^{tot} - c_T\right), \tag{10}$$

where $s_{i,j}^{tot} \equiv \int_{a_{i,j}} s(x,y)\, dxdy$ and the integration is now over the rescaled cell area $a \equiv A / L^2$. Recall that we chose $\sigma(x) = 0$ for $x < 0$, $\sigma(x) = 1$ $x \geq 0$.

There are only two dimensionless groups in the resulting dimensionless system

$$\alpha \equiv hk_s / D, \quad c_T \equiv a\, C_T / C_0^{tot}. \tag{11}$$

The first group characterizes the balance between ligand degradation and transport. The second group is the rescaled threshold in the protease generation function.

To complete the derivation of the discrete model we solve the transport problem for the extracellular ligand. Since the problem is linear, the solution can be evaluated as a superposition of fields due to secretion from individual cells.

Ligand field for a single-cell source

Consider a single ligand-releasing cell placed at the origin of the epithelial layer ($i = 0, j = 0$), secreting the ligands with the dimensionless rate $p_{0,0} = 1$. Then, the resulting ligand field $q(x,y)$ satisfies:

$$\alpha\Delta q - q + \theta_{0,0}(x,y) = 0 \tag{12}$$

where $\theta_{0,0}(x,y) = 1$ everywhere on the surface of the cell placed at the origin and zero everywhere else. The ligand fields computed for a particular set of biophysical parameters for square and hexagonal cells are shown in Figure 2.

Using the two-dimensional cosine transform, the ligand field can be found as:

$$q(x,y) = \frac{4}{\pi^2}\int_0^\infty\int_0^\infty \frac{F(\omega,\lambda)}{\alpha(\omega^2+\lambda^2)+1}\cos(\omega x)\cos(\lambda y)\,d\omega d\lambda \tag{13}$$

Here, $F(\omega,\lambda)$ is the Cosine Transform of $\theta_{0,0}(x,y)$ (see Figure 6A,B, and the discussion in the Appendix). The function $F(\omega,\lambda)$, depends both on the shape and the size of the cell. The expressions for $F(\omega,\lambda)$ for the square and hexagonal-shaped cells are given in the Appendix.

The formula for the ligand field in Equation 13 can be used to evaluate the integrals in the argument of the function specifying the protease production. Specifically, to evaluate the right-hand side of the balance of the cell *ij*, we compute the total amount of ligand over its surface (see equation 10). For a single source of strength $p_{0,0}$, we have:

$$s_{i,j}^{tot} = p_{0,0} \int_{a_{i,j}} q(x,y)dxdy \equiv p_{0,0} I_{i,j} \tag{14}$$

The last expression is a crucial result of this paper, it defines the coupling coefficients for cell communication by secreted ligands. Clearly, $s_{i,j}$ depend only on the relative position between the i,j-th cell and the source. Thus, the same formula can be used to compute the ligand generated by an arbitrary cell .

Cell-cell coupling coefficients

The derived coupling coefficients have a very transparent probabilistic interpretation. Specifically, each coefficient can be interpreted as the fraction of the ligand trajectories that, having started at the cell at the origin, are absorbed by the *i,j*-th cell (see also Conclusions). In addition, the coefficients lead to a number of useful expressions. The number of ligand-receptor complexes on the surface of the i,j-th cell due to the ligand-releasing cell at the origin can be found as:

$$C_{i,j}^{tot} = \int_{A_{i,j}} C(X,Y)dXdY = C_0 L^2 \int_{a_{i,j}} s(x,y)dxdy = \frac{C_0^{tot} L^2}{A} I_{i,j} p_{0,0} \tag{15}$$

where C_0^{tot} is the total number of ligand receptor-complexes on the cell surface when the entire layer is producing ligand at the maximum rate. Hence, to compute the number of complexes due to a single cell, one has to multiply this maximal value (C_0^{tot}) by the interaction coefficient and divide the result by the dimensionless cell area ($a \equiv A/L^2$): $C_{i,j}^{tot} \big/ C_0^{tot} = I_{i,j} \big/ a$.

Using linear superposition, we express the total number of ligand receptor complexes for an arbitrary pattern of protease activity:

$$C_{i,j}^{tot} = \frac{C_0^{tot} L^2}{A} \sum_{m,n} I_{i-m,j-n} p_{m,n} \,, \tag{16}$$

where we used translational symmetry. The analogous equation holds for the extracellular ligand: $s_{ij}^{tot} = \sum_{m,n} I_{i-m,j-n} p_{m,n}$. For arrays of square and hexagonal cells these coefficients are explicitly computed in the Appendix.

Discrete model for cell communication

We now use the coupling coefficients to formulate a discrete model of cell communication. Substituting the expression for $s_{i,j}^{tot}$ into the protease balance we obtain:

$$\frac{dp_{i,j}}{d\tau} = -p_{i,j} + \sigma\left(\sum_{m,n} I_{i-m,j-n} p_{m,n} - c_T \right). \tag{17}$$

Hence, the original system of integrodifferential equations has been reduced to a system of ordinary differential equations (with explicitly available coupling coefficients). As a result, we have a dynamical system that describes the protease dynamics in each cell within the epithelial layer. The model is long-ranged, since the dynamics in each cell depend on the pattern of protease activity in the entire layer. The model is fully discrete, since we resolve individual cells and have "removed" the continuum part of the problem.

Parametric analysis of coupling coefficients

Given the expressions for the interaction coefficients (see Appendix), we can examine their dependence on the biophysical parameters of the original problem. In the case of EGFR signaling in *Drosophila* egg development, the cell area (A) and the height of the gap between the oocyte and follicle cells (h) have been estimated from microscopic images: (h~0.5 μm, A~25 μm^2) (Spradling 1993). The extracellular diffusivity of the ligand (Spitz) and the binding/internalization rate constants can be estimated from the corresponding values in the mammalian EGFR systems. Using these parameters, we present the dependence of the coupling coefficients on the ligand diffusivity and the forward-binding rate constant in Figure 3. Note that we plot the coupling coefficients as functions of the distance between cells. This is done only for convenience in representing discrete data points, of course in the fully discrete context the coupling coefficients are anisotropic (although the degree of anisotropy proves to be rather small both for square and hexagonal cells). Similarly, the lines connecting the points in Figure 3 are used only to guide the eye.

The computation in Figure 3 probes the spatial operation of an autocrine system, a mode of cell-cell signaling where cells can both release and recapture the ligand. The spatial decay of coupling coefficients is controlled by kinetics and transport. The rate of the decay increases with the forward-binding rate constant and decreases with the ligand diffusivity. We find that for the biophysically relevant set of parameters – the geometry of the egg chamber and the transport/kinetic rate constants – the interaction coefficients

decay rapidly as a function of the cell-cell distance. In fact, the interaction between the cells separated by more than 3-4 cell diameters is negligible. This is in line with the conclusions of genetic experiments that can indirectly estimate the spatial range of ligand action *in vivo* (Bergmann and others 2002; Freeman 1997; Peri and others 2002; Stevens 1998).

The rapid decay of the coupling coefficients can be exploited in the computational analysis of the discrete problem, Equation 17. In simulating the arrays of cells, one has to evaluate the coupling only between the finite (and small) number of cells. This greatly simplifies the evaluation of the right-hand side of Equation 17.

Analysis of the positive feedback circuit

We now illustrate the use of our model in a number of computational experiments with the positive feedback circuit, Figure 1. Our computations are directly related to the recent results in *Drosophila* egg development, reviewed in (Amiri and Stein 2002). In one of the experiments, Peri et. al used genetics to permanently activate the protease and hence, the ligand release, in a small (2-4) group of cells within the follicular epithelium (Peri and others 2002). The ligand (Spitz) acts on the cognate receptors (EGFR) on the surfaces of epithelial cells. The authors then followed the level of expression of the gene controlled by the receptor (*pipe*) (Amiri and Stein 2002). It was found that *pipe* was repressed both in the Spitz-releasing cells and in their neighbors. It is well known that ligand-receptor (EGFR/Spitz) binding in this system stimulates the expression of the

ligand-releasing protease (Rhomboid) and that the released ligand (Spitz) can activate the protease in the neighboring cells, Figure 1B,E. So what prevents the perturbation from spreading across the cellular layer? What controls the effect – the strength of ligand release, the extracellular transport, or the size of the perturbation (the number of cells constitutively expressing the protease)? Our computations illustrate how these questions might be addressed within the presented biophysical framework.

First, we construct stable stationary solutions of the discrete problem of cell-cell communication, Equation 17. Let us emphasize that these solutions have no analogoues in the continuous reaction-diffusion models with bistable nonlinearirty. For illustrative purposes, we consider simple three-cell perturbations in the square and hexagonal lattices, Figure 4. In experiments, cells within these clusters expressed the protease independently of ligand/receptor binding. In terms of our model, this means that the protease level in these cells is constant. For the Heaviside nonlinearity used by us, the stable level of the protease can have only two values: the "on" state, for which $p_{i,j} = 1$, and the "off" state, where $p_{i,j} = 0$.

The transition between the two states is induced when the argument of the protease generation function exceeds the critical value given by c_T (Equation 11). The argument, in turn, depends on the pattern of protease activity in the entire cellular layer (see Equation 17). For the cases shown in Figure 4, the condition for the "off→on" transition (ignition) of one of the cells next to the original perturbation can be written as:

$$I_{0,1}(\alpha) + I_{1,1}(\alpha) + I_{-1,1}(\alpha) = c_T \quad \text{(Figure 4A)}$$
$$I_{1,0}(\alpha) + I_{-1,1}(\alpha) + I_{0,1}(\alpha) = c_T \quad \text{(Figure 4B)}$$

These conditions are written for the three-cell perturbation placed at the origin of the cell lattice. For each case, the cell most susceptible to this transition, is marked on the insets of Figure 4A,B. See Appendix for the definition of the indexing schemes.

In writing the "ignition" condition, we keep the dependence of coupling coefficients on α, the dimensionless group combining the kinetic and transport properties (refer to the definition in Table 3). Using this condition, the value of the critical threshold in the right-hand side can be computed for every value of α. This defines an upper boundary of the localized three-cell patterns in Figures 4A,B. Thus, the construction of the stability boundary amounts to evaluating only a small number of coefficients.

Using the definitions of α and c_T (equation 11), we translate these dimensionless groups into the dimensional parameters of reaction transport problem in Equations 1-4. In Figure 4 we plot these boundaries as functions of ligand release rate and the ligand-receptor affinity, the two parameters that have been shown to regulate the operation of autocrine loops in a number of cell culture EGFR systems. In our computations, the range of ligand affinity was dictated by the large amount of binding data available for the EGFR system (Lauffenburger and Linderman 1993; Wiley and others 2003). The rate of ligand release suggested by our computations spans the range attainable in the experiments with cultured autocrine EGFR-expressing cells (DeWitt and others 2001; Dong and others 1999). Note, that at this time there are no quantitative data on ligand release rates *in vivo*.

In addition to static perturbations, such as those used by Peri et al (Peri and others 2002), we can consider the perturbations that transiently activate ligand release in a group of cells. What is the fate of a transient perturbation? Will it decay to zero or persist when the stimulus is turned off? The condition under which a pattern is extinguished (i.e., at least one of the cells within the cluster undergoes the transition to the "off" state) can also be easily formulated as a simple equation for a small group of coupling coefficients. For example,

$$I_{0,0}(\alpha) + I_{1,0}(\alpha) + I_{2,0}(\alpha) = c_T \quad \text{(Figure 4A)}$$
$$I_{0,0}(\alpha) + I_{2,-1}(\alpha) + I_{1,-1}(\alpha) = c_T \quad \text{(Figure 4B)}$$

This equation defines the lower boundaries in the two-parameter diagrams in Figure 5A,B.

To study the evolution of a transient localized perturbation, we simulated the dynamical problem with an initial condition specified by a given pattern of the protease activity. For example, Figure 5 presents three qualitatively different outcomes resulting from activating ligand release in a three-cell cluster, Figure 5A. The ligand fields presented in this figure were generated by first solving the discrete model for the protease pattern, and then using this pattern as the source term in a linear ligand transport problem. For ligand affinities and release rates within the domain of existence of a localized pattern, this perturbation evolves into a stable signaling pattern that is confined to three cells, Figure 5C. This is in marked difference with the analogous continuous system, in which a localized perturbation either decays or results in the onset of signal propagation. Increasing the rate of ligand release leads to overstepping of the upper stability boundary,

Figure 5D. In this case, the localized perturbation acts as a "seed" for an ignition front that travels outwards, leaving the cells in the "on" state. This is similar to the continuous case (Pribyl and others 2003). For low rate of ligand release, the transient activation of protease activity induces only a transient response, Figure 5B. Note, however, that the thresholds of propagation and extinction are both determined by the fully discrete setup (see above).

An interesting feature of the two-parameter diagrams in Figures 4A,B, is the presence of a clear minimum in the dependence of the critical rate of ligand release on the ligand-receptor binding affinity. In terms of the model, it means that the domain of parameters for which the particular localized pattern exists is disconnected. This is illustrated by a one-dimensional cut through the two-parameter diagram, Figure 4C. We verified that overstepping both the left and the right boundaries in this plot generates an ignition front (see the discussion above). The nature of these transitions can be described as follows. For low ligand affinities, binding and transport can not generate a number of ligand-receptor complexes that is necessary for activating the positive feedback. On the other hand, very high binding affinities prevent an efficient transport of ligand. This regime corresponds to the case, when cell-cell coupling coefficients decay very rapidly as a function of cell-cell distance (see Figure 3). In other words, ligand is degraded before it is passed on to the neighbors.

Finally, Figure 4D demonstrates that the effect of the localized perturbation is critically affected by the size of the perturbation. For the examples presented in Figure 4D, the

upper stability boundary that was correlated with the initiation of "ignition" fronts, is negatively correlated with the size of the perturbation. The fact that the stability boundary strongly depends on the size of the perturbation is an immediate consequence of the fact that coupling beyond next-nearest neighbors is important. Experiments with constitutively active ligand release are frequently limited by the ability to control the size of the perturbation (Peri and others 2002). We suggest that the corresponding results should be interpreted with care. In particular, for the same values of binding, signaling, and transport parameters, changing the size of the perturbation can move the system between the regimes of localized and long-range signaling.

Conclusions

We have developed discrete models of cell-cell communication in epithelial layers. In analyzing autocrine and paracrine signals, we consider the molecules, the feedback loops, and the geometry of cell-cell communication that are conserved across species (Casci and Freeman 1999). EGFR system serves as a paradigm for autocrine/paracrine tissue regulation and in multiple developmental, and pathological contexts EGFR is controlled by the positive feedback loop discussed in this paper (Wells 1999). Indeed, the EGFR/Ras/MAPK-mediated feedback from ligand binding to ligand release operates in many mammalian systems (Dent and others 1999; Doraiswamy and others 2000; Gechtman and others 1999; Montero and others 2002). At this time all models of EGFR system are formulated at the level of a single cell (Wiley and others 2003). Our work is aimed at the development of mechanistic models at the tissue level.

One of our main results is the derivation of cell-cell coupling coefficients as a function of geometric, cellular, and molecular parameters of the ligand transport problem. These coefficients provide a quantitative framework for the analysis of cell-cell interactions by diffusing ligands in epithelial layers. Our explicit expressions for the coupling coefficients obtained for particular geometries can be used to estimate the range of cell communication in epithelial layers. Note, however, that our approach – "removing" the continuum part of the problem by slaving it to intracellular variables through the introdiction of cell-cell coupling coefficients - is not limited to periodic arrays of cells of simple shapes and can be applied to arbitrary cell arrangements.

In addition to the general analysis of autocrine signals in epithelial layers, we have analyzed a discrete and nonlinear model of the positive feedback between ligand release and binding. In particular, we found a class of stable stationary solutions in the form of clusters of a few signaling cells. The existence of these solutions is due to the essential discreteness of the considered system. These results can be applied to the EGFR signaling in *Drosophila* oogenesis. This is possible due to the well-characterized "geometry" of cell communication in this problem, and to the availability of molecular and cellular data for the EGFR system. The results on localized patterns can be used to analyze the patterned states generated by the localized activation of ligand release in the follicular epithelium (Pai and others 2000; Peri and others 2002).

While this work has been primarily motivated by the EGFR-mediated cell communication, recent advances in cell biology of developmental signaling pathways enable the formulation of mechanistic models for other systems. Recent data on ligand-receptor affinity in the Wingless pathway can be combined with the spatially resolved measurements of Wingless transport (Dubois and others 2001; Lloyd and others 2002; Pfeiffer and others 2002). This provides a good incentive for the development of transport models that could account for the processes of intracellular ligand trafficking (Entchev and others 2001; Seto and others 2002).

The rapid decay of coupling coefficients suggested by our computations is in line with the conclusions of experimental studies of the EGFR system, both in vitro and vivo. We suggest that, in epithelial layers, many autocrine and paracrine networks may be operating in the regime of "almost" next-nearest neighbor coupling. If, as a result of future quantitative experiments, this turns out to be the case, then modeling of epithelial layers might draw from a large body of mathematical results available for lattice dynamical systems, see (Cahn and others 1998; Chow and others 1998). These results can be used to estimate the velocities of traveling solutions and propagation failure.

Our approach has a number of limitations. While the ligand-limited regime and the "thin-fin" approximation are likely to hold for a large number of developmental contexts, special care has to be paid to assessing the validity of the assumption about the separation of the time scales corresponding to binding and transport and the intracellular variables. New methods have to be developed for the regime when this condition is not satisfied. In

addition, we assumed that the generation of the ligand-releasing protease is a threshold-like function of the current level of ligand-receptor complexes. More complex parameterizations of this dependence can be considered. We verified numerically that similar results are obtained if one uses a (sufficiently sharp) Hill function or more complicated continuous function for the sigmoidal nonlinearity.

Another important issue that needs to be addressed is the effect of the noise on the signaling patterns due to the low number of molecules involved. In fact, a simple calculation shows that for realistic parameters (see Table 1) the number of ligand molecules over a single cell must be of order unity in order for the ligand-limiting regime to be realized. This must therefore be reconciled with the use of the continuous approximation for ligand diffusion (Equation 1). Let us point out, however, that the relevant quantitiy for the signaling patterns here is the number of ligand-receptor complexes per cell $C_{i,j}^{tot}$, which acts as an input to the protease production. In contrast to the number of ligands, the number of complexes turns out to be large: for realistic parameters $C_{i,j}^{tot} \sim 10^3$. This is essentially due to the fact that the average lifetime of the ligand-receptor complexes $\sim (k_e + k_{off})^{-1}$ is much longer than the time scale of ligand-receptor binding $\sim h / k_s$ (see Table 1). Therefore, for these values of $C_{i,j}^{tot}$ the effect of the fluctuations in the number of extracellular ligands will be averaged over times ~ $\sim (k_e + k_{off})^{-1}$ and to the leading order can be neglected. In this sense Equation 1 should be viewed as the equation for the probability density of finding a ligand molecule in a

given infinitesimal volume element. We have performed preliminary Monte-Carlo simulations that also confirm these statements.

Our main goal was to develop a biophysical framework that combines intracellular processes with the information about the kinetics and transport of diffusing signals in epithelial layers. The combination of kinetic models with the detailed information about the subcellular structures has been very successful in the analysis of intracellular events (Slepchenko and others 2002). We argue that a similar approach is critical for the analysis at the tissue level. A rapidly growing number of well characterized developmental systems makes this approach both necessary and feasible (Freeman and Gurdon 2002).

Appendix

Dimensionless model

Rescaling Equations 1 and 4 according to Equations 7 and 8, we obtain:

$$\tau_s \frac{\partial s}{\partial \tau} = \frac{\partial^2 s}{\partial x^2} + \frac{\partial^2 s}{\partial y^2} + \frac{\partial^2 s}{\partial z^2}, \quad \left(\gamma \frac{\partial s}{\partial z} - s \right)\Big|_{z=0} = -(1-\gamma)c - \gamma \sum_{i,j} \theta_{i,j}(x,y) p_{i,j}, \quad \frac{\partial s}{\partial z}\Big|_{z=\alpha} = 0 \quad \text{(A1)}$$

where $\alpha = hk_s / D,\ \gamma = k_e /(k_{off} + k_e),\ \tau_s \equiv Dk_p \big/ k_s^2$. According to this equation, for $\alpha = h / L \ll 1$, the variation of s in the z-direction is negligible. Hence, $s(x, y, y, \tau) \simeq \overline{s}(x, y, \tau)$. Using this fact and averaging Equation A1 over the vertical coordinate, we get approximately:

$$\tau_s \frac{\partial \overline{s}}{\partial \tau} = \frac{\partial^2 \overline{s}}{\partial x^2} + \frac{\partial^2 \overline{s}}{\partial y^2} + \frac{1}{\alpha} \frac{\partial s}{\partial z}\Big|_0^{\alpha}$$

Combining this with the rescaled versions of Equations 2, 3 and using the boundary conditions in Equation A1, we get:

$$\tau_s \frac{\partial s}{\partial \tau} = \frac{\partial^2 s}{\partial x^2} + \frac{\partial^2 s}{\partial y^2} - \frac{1}{\alpha\gamma} \left(s - (1-\gamma)c - \gamma \sum_{i,j} \theta_{i,j}\left(x,y\right) p_{i,j} \right) \quad \text{(A2)}$$

$$\tau_c \frac{\partial c}{\partial \tau} = s - c \quad \text{(A3)}$$

$$\frac{dp_{i,j}}{d\tau} = -p_{i,j} + \sigma \left(\int_{a_{i,j}} s\left(x,y\right) dxdy - c_T \right) \quad \text{(A4)}$$

where $c \equiv C / C_0$. Equations A2-4 contain four dimensionless parameters: $\alpha,\ \tau_s, \tau_c, c_T$ For the thin-fin approximation in Equation A1, α (i.e. ratio of the geometrical and the dynamical length) has to be small. This condition is satisfied for the typical parameter set

used in the model analysis (see Table 3). Furthermore the relative time scales of extracellular ligand and ligand-receptor complexes are small: $\tau_c \ll 1$ and $\tau_s \ll 1$; see Table 3. The steady-state approximation for these variables leads to Equations 9,10 (in the original scaling).

Coupling coefficients for square cells

Now we will compute the coupling coefficients $I_{m,n}$ for square cells of size L_x.

Let $F(\omega,\lambda)$, be the Cosine Transform of $\theta_{0,0}(x,y)$:

$$F(\omega,\lambda) = \frac{\sin(\omega l/2)\sin(\lambda l/2)}{\omega\lambda} \tag{A5}$$

where $l = L_x / L$ is the dimensionless cell width (see Fig. 6A). The coupling coefficients can then be found via integration of Equations 13 and 15. After tedious but straightforward algebra, we obtain:

$$I_{m,n} \equiv \int_0^\infty\int_0^\infty \frac{16\cos(ln\lambda)\cos(lm\omega)\sin^2(l\lambda/2)\sin^2(l\omega/2)}{\pi^2\lambda^2\omega^2(\alpha(\lambda^2+\omega^2)+1)} d\omega d\lambda \tag{A6}$$

where *m* and *n* are the position indices that determine the locations of the *m,n*–th cells in the lattice (see Fig. 6C).

Coupling coefficients for hexagonal cells

It is not difficult to check that for the hexagonal cells with dimensionless width $2v = 2L_v / L$, the cosine transform $F(\omega,\lambda)$ of $\theta_{0,0}$ is given by

$$F(\omega,\lambda)=\frac{2v\left(\lambda r\left(\cos(\lambda r)-\cos(\lambda r/2)\cos(\omega v)\right)+2v\omega\sin(\lambda r/2)\sin(\omega v)\right)}{4v^2\lambda\omega^2-r^2\lambda^3} \quad \text{(A7)}$$

where $r=2v/\sqrt{3}$ is the side of the hexagon (see Fig 6B).

From equation 14, the interaction coefficient is $I_{m,n}\equiv\int_{a_{m,n}} q(x,y)\,dxdy$, where the function $q(x,y)$ is defined by equation 13. To compute the coupling coefficients, we integrate this expression over the *m,n*–th cell. This requires evaluating the integral $\int_{a_{m,n}}\cos(\omega x)\cos(\lambda y)dxdy$. With the indexing scheme (see Figure 6D), the position of cell centers on the hexagonal lattice is given by

$$x=mv,\quad y=3rn+3rm/2 \quad \text{(A8)}$$

Then, after a straightforward calculation the integral $\int_{a_{m,n}}\cos(\omega x)\cos(\lambda y)dxdy$ for the *m,n*–th cell can be written as:

$$\int_{a_{m,n}}\cos(\omega x)\cos(\lambda y)dxdy=\frac{8v\cos(3(m+2n)r\lambda/2)\cos(mv\omega)\left(r\lambda\left(\cos(r\lambda)-\cos(r\lambda/2)\cos(v\omega)\right)+2v\omega\sin(r\lambda/2)\sin(v\omega)\right)}{4v^2\lambda\omega^2-r^2\lambda^3} \quad \text{(A9)}$$

This expression can be substituted into Equations 13 and 14. After a long calculation, the coupling coefficients become:

$$I_{m,n}=\int_0^\infty\int_0^\infty\frac{64v^2\cos(3(m+2n)r\lambda/2)\cos(mv\omega)\left(r\lambda\left(\cos(r\lambda)-\cos(r\lambda/2)\cos(v\omega)\right)+2v\omega\sin(r\lambda/2)\sin(v\omega)\right)^2}{\pi^2\lambda^2(r^2\lambda^2-4v^2\omega^2)^2(\alpha(\lambda^2+\omega^2)+1)}d\omega d\lambda \quad \text{(A10)}$$

General comments

The integrals given by equations A6 and A10 can be easily computed numerically. We have used adaptive integration routines in Mathematica and MATLAB for this purpose. The computation of a single coefficient takes several seconds on a very modest PC. Given the fact that coupling coeffients decay rather quickly as a function of the lattice indices, the vectorfield for the discrete problem is constructed very efficiently. The numerical integration of this vectorfield was done using standard MATLAB routines for ODEs. In the current form, the coupling coefficients depend on the dimensionless cell size (l, or v and r) and $\alpha = k_s h / D$, a dimensionless parameter inherited from the original three-dimensional problem. By rescaling the variables of integration in the final expressions (Equations A6 and A10), that $\mathrm{I}_{m,n} = \alpha f(m,n,l/\sqrt{\alpha})$. Thus up to a constant, the integrals in A6 and A10 depend on a single dimensionless parameter $l/\sqrt{\alpha}$. Returning to the dimensional parameters, we find that $l/\sqrt{\alpha}$ is equal to the cell size, l (or v and r), normalized by the length scale for ligand variations along the surface $\sqrt{Dh/k_s}$. The original cell communication system operates in a discrete regime when the ratio of these length scales is greater than one. The cells are essentially uncoupled for very large values of $l/\sqrt{\alpha}$. Small values of $l/\sqrt{\alpha}$ correspond to the continuum regime.

ACKNOWLEDGEMENT

The authors thank L. Batsilas (Princeton) for his critical reading of the manuscript. This work was supported by the NSF grant DMS-0211864.

References

Amiri A, Stein D. 2002. Dorsoventral patterning: a direct route from ovary to embryo. Curr Biol 12(15):R532.

Barkai N, Shilo BZ. 2002. Modeling pattern formation: counting to two in the Drosophila egg. Curr Biol 12(14):R493.

Bergmann A, Tugentman M, Shilo B, Steller H. 2002. Regulation of Cell Number by MAPK-Dependent Control of Apoptosis. A Mechanism for Trophic Survival Signaling. Dev Cell 2(2):159-170.

Bolouri H, Davidson EH. 2002. Modeling transcriptional regulatory networks. Bioessays 24(12):1118-29.

Brand AH, Perrimon N. 1993. Targeted gene expression as a means of altering cell fates and generating dominant phenotypes. Development 118(2):401-15.

Burke P, Schooler K, Wiley HS. 2001. Regulation of epidermal growth factor receptor signaling by endocytosis and intracellular trafficking. Moll Cell Biol 12(6):1897-910.

Cahn JW, Mallet-Paret J, Van Vleck ES. 1998. Traveling wave solutions for systems of ODEs on a two-dimensional spatial lattice. SIAM J Appl Math 59(2):455-493.

Carmena A, Buff E, Halfon MS, Gisselbrecht S, Jimenez F, Baylies MK, Michelson AM. 2002. Reciprocal regulatory interactions between the Notch and Ras signaling pathways in the Drosophila embryonic mesoderm. Dev Biol 244(2):226-42.

Casci T, Freeman M. 1999. Control of EGF receptor signalling: Lessons from fruitflies. Cancer Metastasis Rev 18:181-201.

Chow SN, Mallet-Paret J, Shen WX. 1998. Traveling waves in lattice dynamical systems. Journ Diff Equations 149(2):248-91.

Collier JR, Monk NA, Maini PK, Lewis JH. 1996. Pattern formation by lateral inhibition with feedback: a mathematical model of delta-notch intercellular signalling. J Theor Biol 183(4):429-46.

Dent P, Reardon D, Park J, Bowers G, Logsdon C, Valerie K, Schmidt-Ullrich R. 1999. Radiation-induced release of transforming growth factor alpha activates the epidermal growth factor receptor and mitogen-activated protein kinase pathway in carcinoma cells, leading to increased proliferation and protection from radiation-induced cell death. Molecular biology of the cell 10(8):2493-2506.

DeWitt A, Dong J, Wiley H, Lauffenburger D. 2001. Quantitative analysis of the EGF receptor autocrine system reveals cryptic regulation of cell response by ligand capture. J Cell Sci 114:2301-13.

Dong JY, Opresko LK, Dempsey PJ, Lauffenburger DA, Coffey RJ, Wiley HS. 1999. Metalloprotease-mediated ligand release regulates autocrine signaling through the epidermal growth factor receptor. Proceedings Of The National Academy Of Sciences Of The United States Of America 96:6235-6240.

Dong JY, Wiley, H. S. 1999. Trafficking and proteolytic release of epidermal growth factor receptor ligands are modulated by their membrane-anchoring domains. Journal Of Biological Chemistry 275:557-564.

Doraiswamy V, Parrot J, Skinner M. 2000. Expression and action of transforming growth factor alpha in normal ovarian surface epithelium and ovarian cancer. Biol Reprod 63(3):789-96.
Dubois L, Lecourtois M, Alexandre C, Hirst E, Vincent JP. 2001. Regulated endocytic routing modulates wingless signaling in Drosophila embryos. Cell 105(5):613-24.
Duffy J, Harrison D, Perrimon N. 1998. Identifying loci required for follicular patterning using directed mosaics. Development 125(12):2263-71.
Dyson S, Gurdon JB. 1998. The interpretation of position in a morphogen gradient as revealed by occupancy of activin receptors. Cell 93(4):557-68.
Entchev E, Schwabedissen A, Gonzalez-Gaitan M. 2001. Gradient formation of the TGF-beta homolog Dpp. Cell 103(6):981-91.
Ferrell J. 1997. How responses get more switch-like as you move down a protein kinase cascade. Trends Biochem Sci 22(8):288-9.
Freeman M. 1997. Cell determination strategies in the Drosophila eye. Development 124(2):261-70.
Freeman M. 2000. Feedback control of intercellular signalling in development. Nature 408:6810.
Freeman M, Gurdon JB. 2002. Regulatory principles of developmental signaling. Annu Rev Cell Dev Biol 18:515-539.
Gechtman Z, Alonso JL, Raab G, Ingber DE, Klagsbrun M. 1999. The shedding of membrane-anchored heparin-binding epidermal- like growth factor is regulated by the Raf/mitogen-activated protein kinase cascade and by cell adhesion and spreading. Journal Of Biological Chemistry 274:28828-28835.
Hasty J, McMillen D, Collins JJ. 2002. Engineered gene circuits. Nature 420(6912):224-30.
Hatini V, DiNardo S. 2001. Divide and conquer: pattern formation in Drosophila embryonic epidermis. Trends Genet 17(10):574-9.
Hogan B. 1999. Morphogenesis. Cell 96:225-233.
Hsu T, McRackan D, Vincent TS, Gert de Couet H. 2001. Drosophila Pin1 prolyl isomerase Dodo is a MAP kinase signal responder during oogenesis. Nat Cell Biol 3(6):538-43.
Lander AD, Nie W, Wan FY. 2002. Do morphogen gradients arise by diffusion? Dev Cell 2(6):785-96.
Lauffenburger DA, Linderman JJ. 1993. Receptors: models for binding, trafficking, and signalling. New York: Oxford University Press.
Lloyd TE, Atkinson R, Wu MN, Zhou Y, Pennetta G, Bellen HJ. 2002. Hrs regulates endosome membrane invagination and tyrosine kinase receptor signaling in Drosophila. Cell 108(2):261-9.
Meir E, von Dassow G, Munro E, Odell GM. 2002. Robustness, flexibility, and the role of lateral inhibition in the neurogenic network. Curr Biol 12(10):778-86.
Monk NAM. 1998. Restricted-range gradients and travelling fronts in a model of juxtacrine cell relay. Bull Math Biol 60(5):901-918.
Montero JC, Yuste L, Diaz-Rodriguez E, Esparis-Ogando A, Pandiella A. 2002. Mitogen-activated protein kinase-dependent and -independent routes control shedding of transmembrane growth factors through multiple secretases. Biochem J 363(2):211-21.

Nilson LA, Schupbach T. 1999. EGF receptor signaling in Drosophila oogenesis. Curr Top Dev Biol 44:203-243.
Othmer HG, Scriven LE. 1971. Instability and dynamic pattern in cellular networks. Journal of Theoretical Biology 32(3):507-537.
Owen MR, Sherratt JA, Myers SA. 1999. How far can a juxtacrine signal travel? Proc Roy Soc, Ser. B 266(1419):579-585.
Owen MR, Sherratt JA, Wearing HJ. 2000. Lateral induction by juxtacrine signaling is a new mechanism for pattern formation. Dev Biol 217(1):54-61.
Pai L, Barcelo G, Schupbach T. 2000. D-cbl, negative regulator of the Egfr pathway, is required for dorsoventral patterning in Drosophila oogenesis. Cell 103(1):51-61.
Peri F, Bokel C, Roth S. 1999. Local Gurken signaling and dynamic MAPK activation during Drosophila oogenesis. Mech Dev 81:75-88.
Peri F, Technau M, Roth S. 2002. Mechanisms of Gurken-dependent pipe regulation and the robustness of dorsoventral patterning in Drosophila. Development 129(12):2965-75.
Pfeiffer S, Ricardo S, Manneville JB, Alexandre C, Vincent JP. 2002. Producing cells retain and recycle wingless in Drosophila embryos. Curr Biol 12(11):957-62.
Pribyl M, Muratov CB, Shvartsman SY. 2003. Long-range signal transmission in autocrine relays. Biophys J 84:883-896.
Ruohola-Baker H, Grell E, Chou TB, Baker D, Jan L, Jan YN. 1993. Spatially localized rhomboid is required for establishing the dorsal-ventral axis in Drosophila oogenesis. Cell 73(5):953-65.
Sapir A, Schweitzer R, Shilo BZ. 1998. Sequential activation of the EGF receptor pathway during Drosophila oogenesis establishes the dorsoventral axis. Development 125:191-200.
Seto ES, Bellen HJ, Lloyd TE. 2002. When cell biology meets development: endocytic regulation of signaling pathways. Genes Dev 16(11):1314-36.
Shilo B. 2001. The organizer and beyond. Cell 106(1):17-22.
Shvartsman SY, Muratov CB, Lauffenburger DA. 2002. Modeling and computational analysis of EGF receptor-mediated cell communication in Drosophila oogenesis. Development 129(11):2577-2589.
Slepchenko BM, Schaff JC, Carson JH, Loew LM. 2002. Computational cell biology: spatiotemporal simulation of cellular events. Annu Rev Biophys Biomol Struct 31:423-41.
Smolen P, Baxter DA, Byrne JH. 2000. Modeling transcriptional control in gene networks--methods, recent results, and future directions. Bull Math Biol 62(2):247-92.
Spradling AC. 1993. Developmental Genetics of oogenesis. The development of Drosophila Melanogaster. Plainview: Cold Spring Harbor Laboratory Press. p 1-70.
Stevens L. 1998. Twin Peaks: Spitz and Argos star in patterning of the Drosophila egg. Cell 95:291-294.
Urban S, Lee JR, Freeman M. 2002. A family of Rhomboid intramembrane proteases activates all Drosophila membrane-tethered EGF ligands. EMBO J 21(16):4277-86.

Van Buskirk C, Schupbach T. 1999. Versatility in signaling: multiple responses to EGF receptor activation during Drosophila oogenesis. Trends in Cell Biology 9:1-4.
von Dassow G, Meir E, Munro EM, Odell GM. 2000. The segment polarity network is a robust developmental module. Nature 406(6792):188-92.
Wasserman JD, Freeman M. 1998. An autoregulatory cascade of EGF receptor signaling patterns the Drosophila egg. Cell 95:355-364.
Wells A. 1999. EGF receptor. Int J Biochem Cell Biol 31:637-643.
Wiley HS, Shvartsman SY, Lauffenburger DA. 2003. Computational modeling of the EGF receptor system: a paradigm for systems biology. Trends Cell Biol 13(1).

TABLE 1 MODEL PARAMETERS

Parameter	Description	Typical value
A	cell surface area	2.5×10^{-7} cm^2
L_x	cell width (squares)	5×10^{-4} cm
$2L_v$	cell width (hexagons)	5×10^{-4} cm
D	ligand diffusivity	1×10^{-7} cm^{2}s^{-1}
h	height of the extracellular medium	5×10^{-5} cm
k_e	ligand-induced internalization rate constant	0.1 min^{-1}
k_{on}	receptor/ligand association constant	0.1 nM^{-1}min^{-1}
k_{off}	receptor/ligand complex dissociation constant	0.1 min^{-1}
k_p	protease degradation rate constant	0.03 min^{-1}
$k_s = k_e k_{on} R_0 / \left(k_e + k_{off} \right)$	ligand degradation constant	5×10^{-5} cm s^{-1}
$Q_s = g_r g_p / k_p$	rate of ligand release per cell	500 molecules/cell/min
R_0	number of receptors per cell	1×10^4 receptors/cell
C_T	threshold for activating the positive feedback	500 complexes/cell

TABLE 2 MODEL VARIABLES

Variable	Description
S	ligand concentration
C	ligand-receptor complex surface concentration
$C_{i,j}^{tot}$	total number of complex molecules over the cell
$P_{i,j}$	number of active protease molecules per cell
t	time
$X,\ Y$	coordinates in the plane of the epithelium
Z	transverse coordinate
$s \equiv S/S_0$	dimensionless ligand concentration
$c \equiv C/C_0$	dimensionless ligand-receptor complex surface concentration
$c_{i,j}^{tot} \equiv C_{i,j}^{tot} \Big/ \left(C_0 L^2\right)$	dimensionless total number of complex molecules over the cell *ij*
$p_{i,j} \equiv P_{i,j}/P_0$	dimensionless number of active protease molecules per cell
$\tau \equiv tk_p$	dimensionless time
$x \equiv X/L,\ y \equiv Y/L$	dimensionless spatial variable

TABLE 3 DIMENSIONLESS PARAMETERS

Variable	Description	Typical value
$\alpha \equiv hk_s/D$	Damköhler number	2.768×10^{-2}
$c_T \equiv aC_T/C_0^{tot} = C_T k_e a/Q_s$	dimensionless threshold in the sigmoidal nonlinearity	
$\tau_c \equiv k_p/\left(k_{off}+k_e\right)$	relative time scale of binding and trafficking	0.15
$\tau_s \equiv Dk_p/k_s^2$	relative time scale of the ligand transport	1.632×10^{-2}
$a \equiv A/L^2$	dimensionless cell surface area	

TABLE 4 SCALING FACTORS

Variable	Description
$S_0 \equiv g_r g_p \big/ \left(A k_p k_s \right)$	ligand concentration
$C_0 \equiv g_r g_p \big/ \left(A k_p k_e \right)$	ligand-receptor complex surface concentration
$C_0^{tot} \equiv C_0 A$	total number of complex molecules over a cell
$P_0 \equiv g_p \big/ k_p$	number of active protease molecules per cell
$L \equiv D \big/ k_s$	the dynamic length scale

FIGURE CAPTIONS

Figure 1 (A) The geometry of the problem is motivated by cell communication in *Drosophila* oogenesis. Epithelial cells cover the large oocyte. EGF receptors areuniformly distributed across the epithelial layer and are absent on the surface of the oocyte. (B) Ligands diffuse in a thin gap between the epithelial layer and a reflective surface. (C) Two model layers considered in this paper – periodic arrays of squares and hexagons. (D) Main processes in ligand binding and transport. (E) Ligand binding stimulates ligand release. Receptor activation leads to the degradation of a factor inhibiting the transcription of the ligand-releasing protease. In the absence of inhibition, the protease is synthesized and generates the secreted ligand.

Figure 2 The steady state ligand field due to a single ligand-releasing cell. (A) Square cells, $L_x = 5 \times 10^{-4}$ cm. (B) Hexagonal cells, $2L_v = 5 \times 10^{-4}$ cm. Other parameters: $h = 5 \times 10^{-5}$ cm, $k_e = 0.1$ min^{-1}, $k_{off} = 0.1$ min^{-1}, $R_0 = 1\times10^4$ molecules/cell surface, $D = 1\times10^{-7}$ cm^{2}s^{-1}, $k_{on} = 0.1$ nM^{-1}min^{-1}, $Q_s = 100$ molecules/cell/min. The fields were computed by solving Equation 12 using an adaptive mesh finite element package (FEMLAB).

Figure 3 Normalized coupling coefficients (C_k^{tot}/C_0^{tot}, see text for details) plotted as a function of cell-cell distance, k, defined as the ratio of the Euclidian distance divided by the cell size. (A) Effect of ligand-receptor affinity k_{on} (square cells, $L_x = 5 \times 10^{-4}$ cm, $D = 1\times10^{-7}$ cm^{2}s^{-1}). (B) Effect of ligand diffusivity D (hexagonal cells, $2L_v = 5 \times 10^{-4}$ cm, $k_{on} = 0.1$ nM^{-1}min^{-1}). All other parameters as in Figure 2.

Figure 4 Stable localized patterns generated by the positive feedback. (A,B) Existence of the localized three-cell patterns for squares (A) and hexagons (B) as a function of ligand release rate and ligand/receptor affinity. The shaded area corresponds to the stable localized pattern. Crossing the upper boundary ignites the neighboring cells. Crossing the lower boundary leads to the extinction of the pattern. (C) A one-dimensional cut (Q_s = 300 molecules/cell/minute) through the diagram in (A) showing the disconnected region

of existence of the localized pattern. Localized patterns are realized both for low and high ligand-receptor affinities. (D) Critical rate of ligand release necessary to destabilize the localized pattern as a function of the number of cells in it, k_{on} = 0.1 $nM^{-1}min^{-1}$. (A-D): C_T = 500 molecules. Other parameters as in Figure 2.

Figure 5 Response of a cellular layer to a localized perturbation in protease release. (A) The structure of the perturbation. (B-D) The ligand fields induced by the perturbation computed for different ligand-release rates. (B) Q_s = 100 molecules/cell/min. Ligand field 40 mins after the perturbation. The perturbation decays.(C) Q_s = 200 molecules/cell/min. The perturbation generates a stable pattern of the same structure. (D) Q_s = 300 molecules/cell/min. The perturbation generates an "ignition" wave (see text for details). All parameters as in Figure 4A.

Figure 6 (A) Solution of equation 12 for the square cells was derived on the two-dimensional semi-infinite domain with the origin in the center of the square. The dimensionless area of the square is a=l^2. (B) Solution of equation 12 for the hexagons was derived on the two-dimensional semi-infinite domain with origin in the center of the hexagon. The dimensionless area of the hexagon is a=$3\times r\times v$. (C) Indexing used for the computation of coupling coefficients for square cells. (D) Indexing used for the computation of coupling coefficients for hexagonal cells.

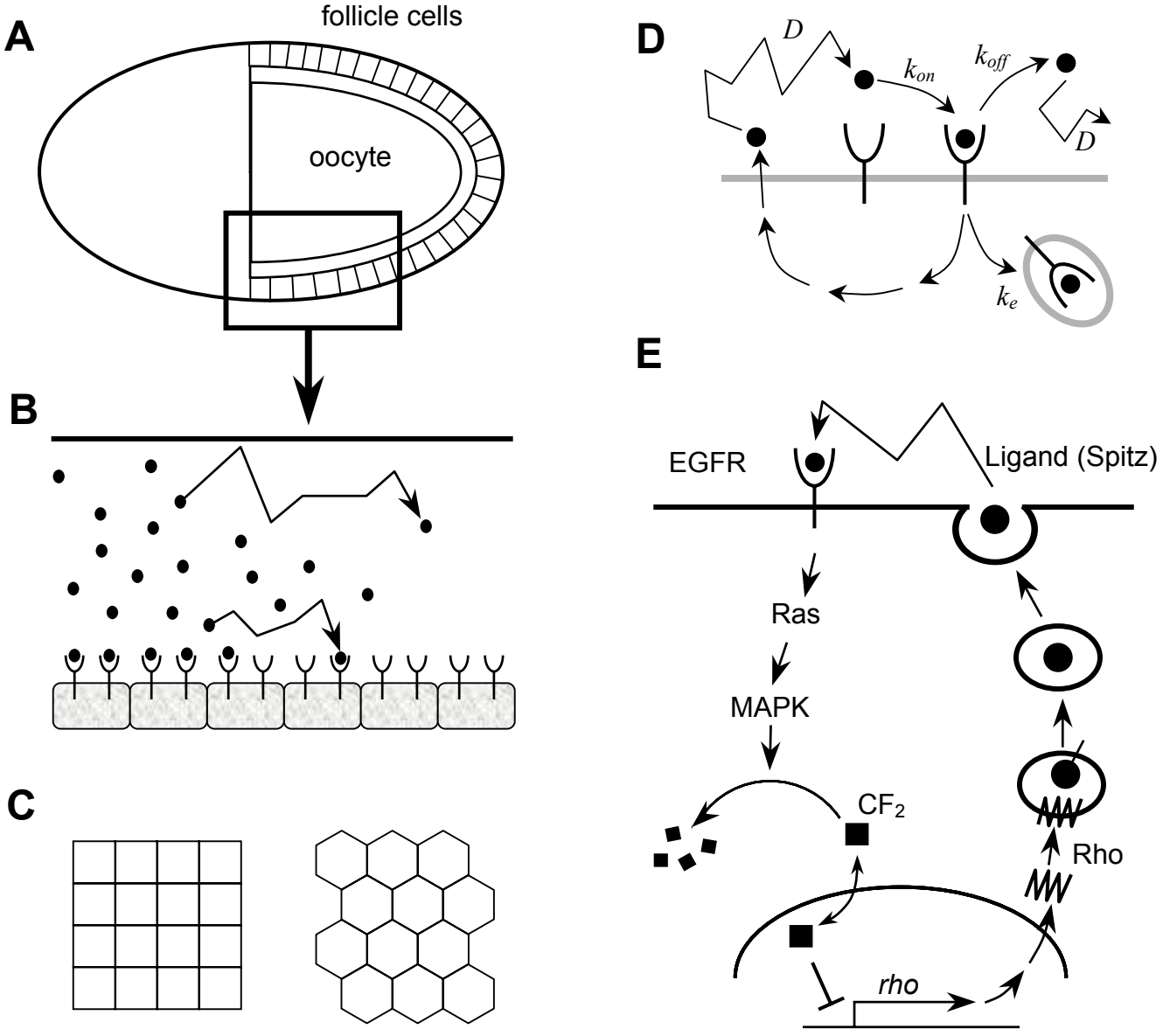
A
follicle cells
oocyte
B
C
D
D
k_{on}
k_{off}
D
k_e
E
EGFR
Ligand (Spitz)
Ras
MAPK
CF_2
Rho
rho

FIGURE 1

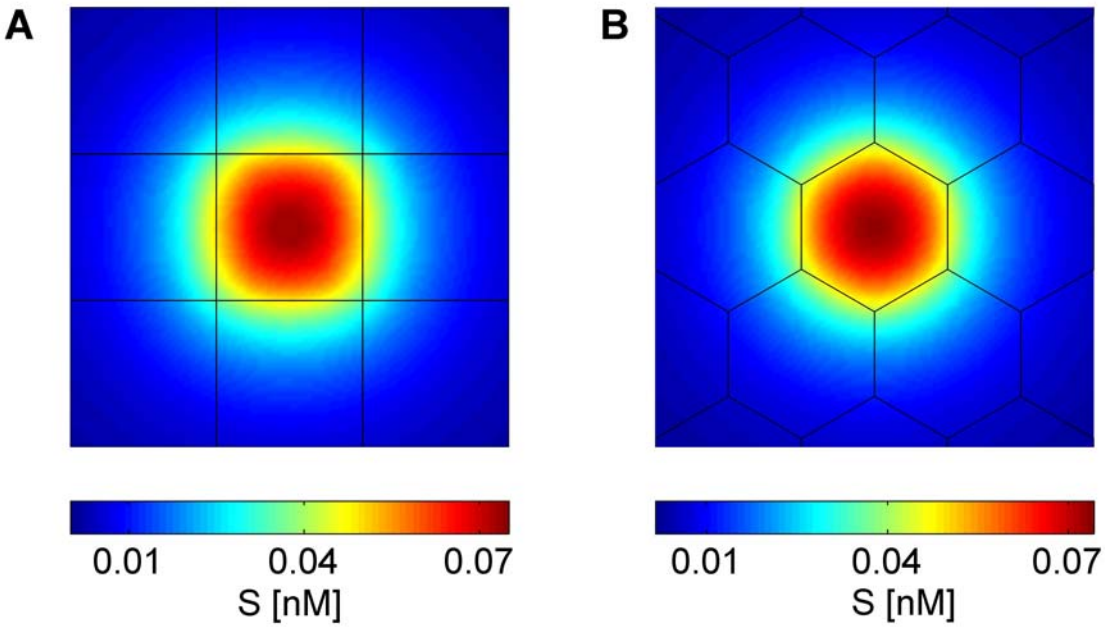

FIGURE 2

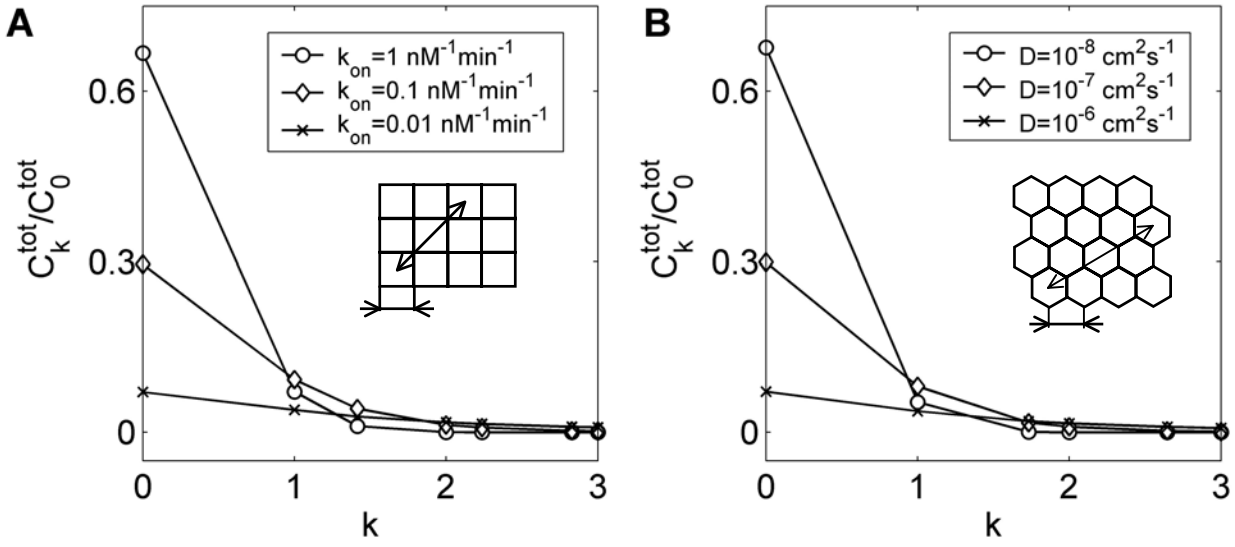
A
B
k_{on}=1 $nM^{-1}min^{-1}$
k_{on}=0.1 $nM^{-1}min^{-1}$
k_{on}=0.01 $nM^{-1}min^{-1}$
D=10^{-8} cm^2s^{-1}
D=10^{-7} cm^2s^{-1}
D=10^{-6} cm^2s^{-1}
C_k^{tot}/C_0^{tot}
0.6
0.3
0
0
1
2
3
k

FIGURE 3

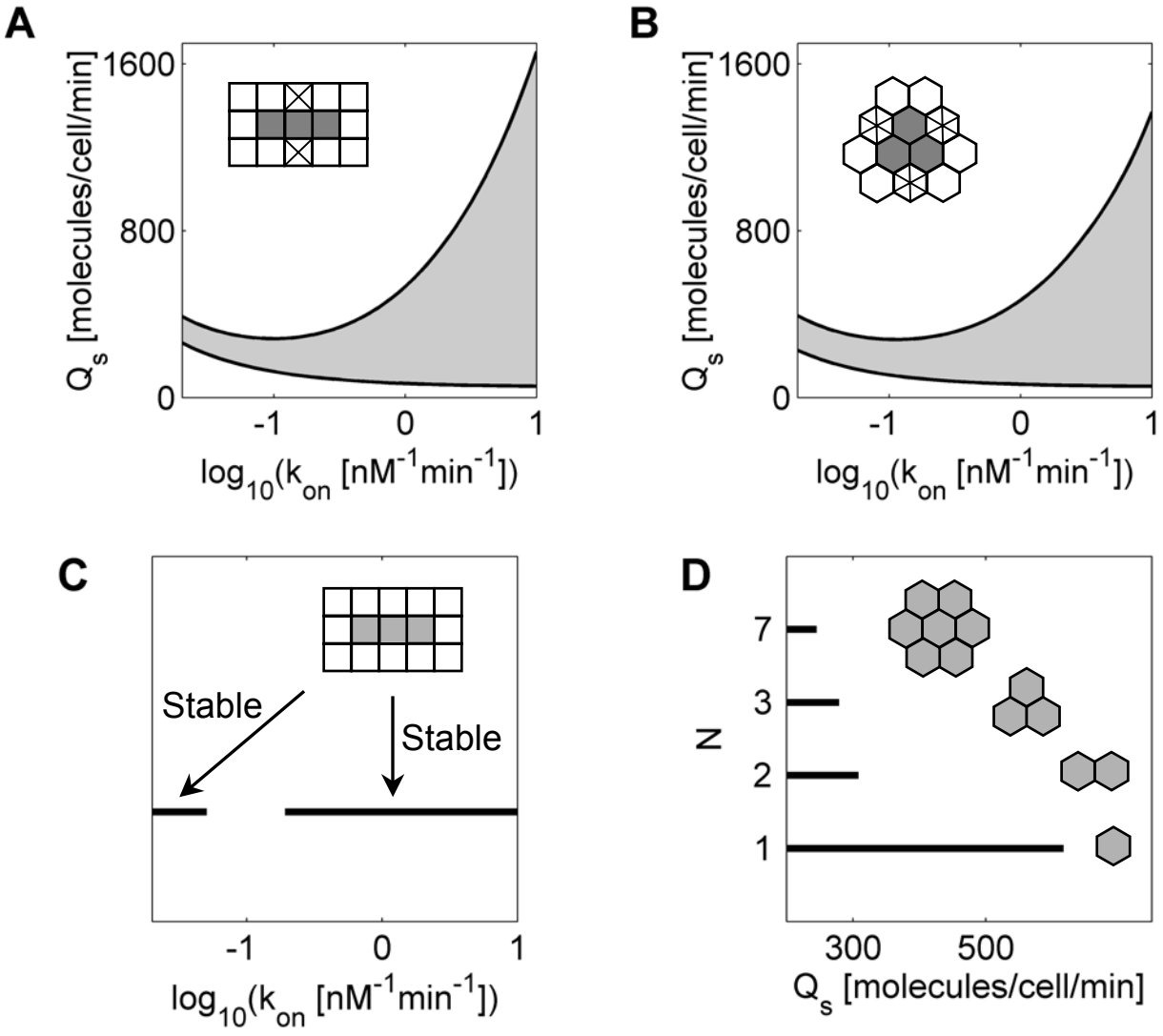
A
B
C
D
1600
800
0
-1
0
1
Q_s [molecules/cell/min]
$\log_{10}(k_{on}$ [$nM^{-1}min^{-1}$])
Stable
Stable
N
7
3
2
1
300
500
Q_s [molecules/cell/min]

FIGURE 4

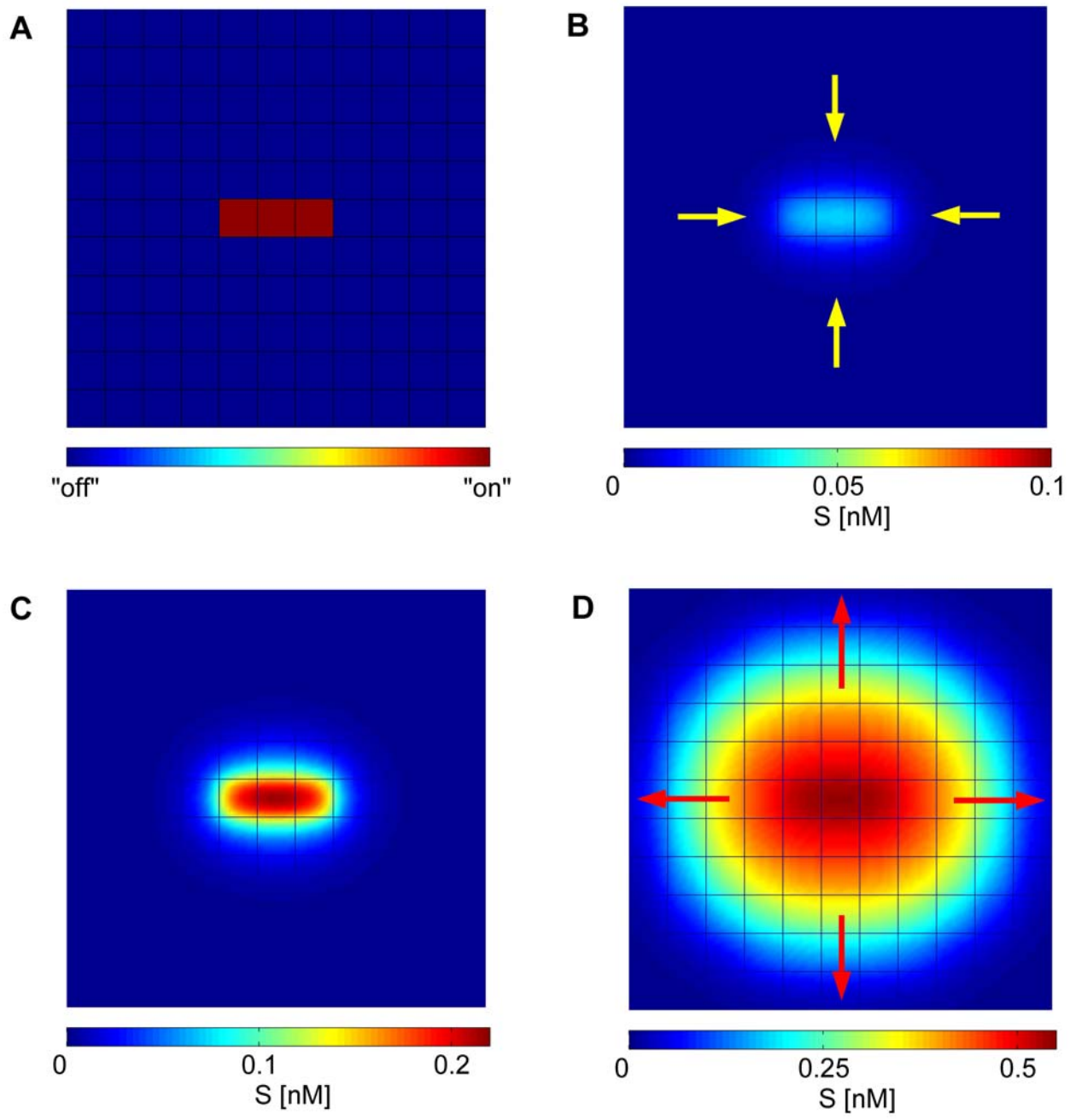

FIGURE 5

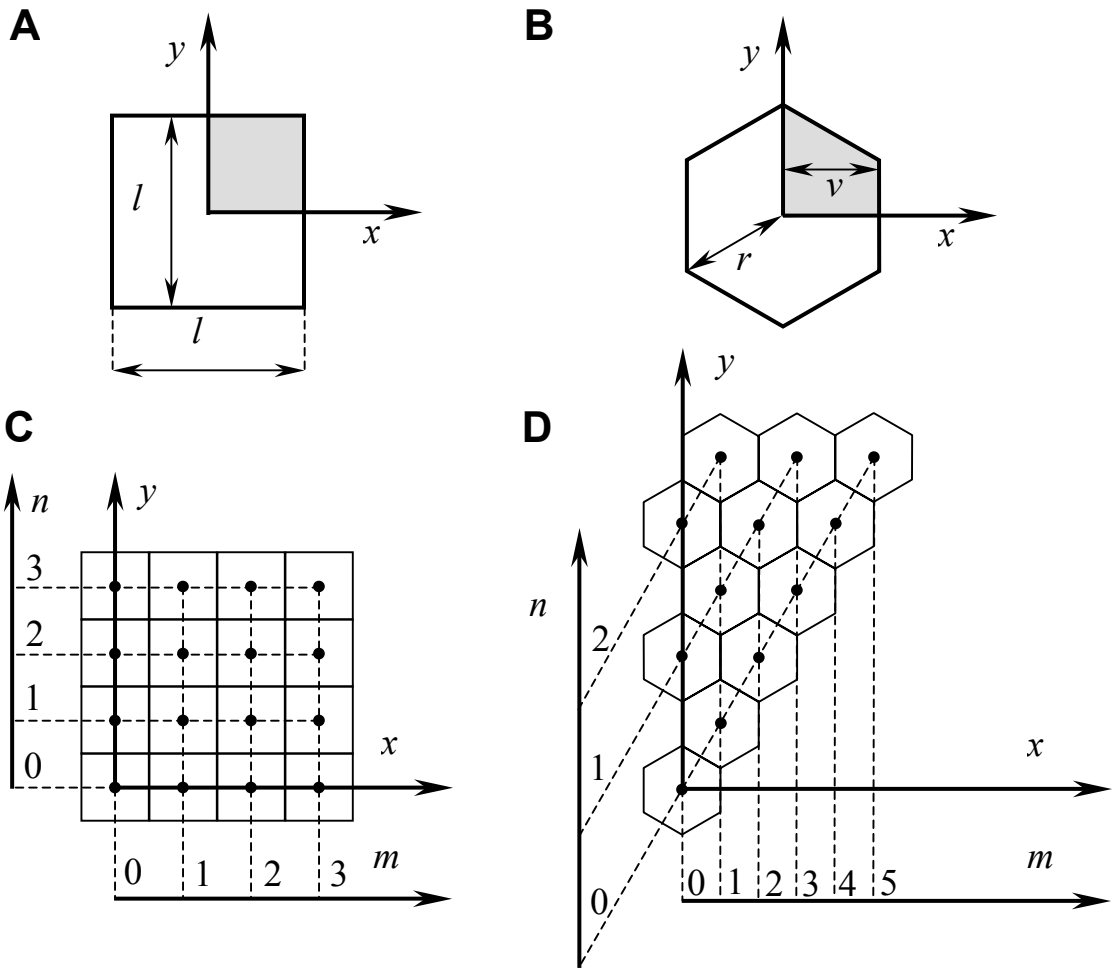

FIGURE 6